MOLECULAR IMAGING AND BIOLOGY

Mol Imaging Biol (2019) 21:140–148
DOI: 10.1007/s11307-018-1219-6

Published Online: 4 June 2018

RESEARCH ARTICLE

Spatial Patterns of Hypometabolism and Amyloid Deposition in Variants of Alzheimer's Disease Corresponding to Brain Networks: a Prospective Cohort Study

Ying Wang,[1] Zhihong Shi,[2] Nan Zhang,[3] Li Cai,[1] Yansheng Li,[1] Hailei Yang,[1] Shaobo Yao,[1] Xiling Xing,[1] Yong Ji,[2] Shuo Gao[1]

[1]*Department of PET-CT Diagnostic, Tianjin Medical University General Hospital, 154 Anshan Road, Heing District, Tianjin, 300052, China*
[2]*Tianjin Key Laboratory of Cerebrovascular and Neurodegenerative Diseases, Tianjin Huanhu Hospital, Tianjin, China*
[3]*Department of Neurology, Tianjin Medical University General Hospital, Tianjin Neurological Institute, Tianjin, China*

Abstract

Purpose: To identify the most vulnerable network among typical and three variants of Alzheimer's disease (AD) and to link amyloid-β (Aβ) deposition and downstream network dysfunction.

Procedures: In this study, 38 typical AD, 11 frontal variants, 8 logopenic variants, 6 posterior variants, and 20 normal controls were enrolled. 2-(4′-[^{11}C] Methylaminophenyl)-6-hydroxybenzothiazole ([^{11}C]PIB) and 2-deoxy-2-[^{18}]fluoro-D-glucose ([^{18}F]FDG) positron emission tomography (PET) imaging were performed. Voxel-wise statistical analysis was used for [^{18}F]FDG analysis, whereas two-sample *t* test was performed between each AD group and control group. Moreover, the goodness of fit (GOF) of *t*-maps with brain functional network templates was assessed, and the most vulnerable network in each phenotypic of AD was chosen as volume of interests (VOIs). [^{11}C]PIB binding potential (BP_{ND}) of VOIs were generated by using PMOD software. In addition, statistical analysis of BP_{ND} among four types of AD in each specific network was calculated by SPSS software.

Results: The hypometabolism patterns indicated that in typical and frontal variants of AD, the most vulnerable network was the left executive control network (GOF score = 4.3, 5.0). For the logopenic variant, the highest GOF score (1.9) belonged to the auditory network. For the posterior variant, the higher visual network was the most vulnerable (GOF score = 6.0). The [^{11}C]PIB BP_{ND} showed that there were no significant differences ($p > 0.05$) among AD groups within the specific networks.

Conclusion: The phenotypic diversity of AD correlates with specific functional network failure; however, Aβ plaques do not associate with specific network vulnerability.

Key words: Alzheimer's disease, Amyloid-β, [^{18}F]FDG, [^{11}C]PIB, Positron-emission tomography

Introduction

Alzheimer's disease (AD) represents a phenotypically diverse group of syndromes that is underpinned by a

Correspondence to: Shuo Gao; *e-mail:* dr_shuogao@hotmail.com

common pathology. AD can present as a typically amnestic form, as well as variant syndromes. Typical AD (TAD) presents over the age of 65 years as an insidious deterioration in episodic, autobiographical, and topographical memory. In general, a stereotypical pattern of cognitive impairment is observed, starting with encoding new memories and inevitably progressing to involve diverse cognitive deficits [1]. Previous studies have shown that this typical amnestic clinical syndrome is associated with a characteristic topographic spread of molecular pathologies [2, 3], and early metabolic reductions in the lateral temporoparietal regions and the retrosplenial cortex prior to involving the frontal regions [4]. The precise definitions for variants of AD presentations have been published in the International Working Group-2 (IWG-2) criteria, and include posterior cortical atrophy (PCA, visual variant of AD), logopenic variant primary progressive aphasia (LPA, a language variant of AD), and a frontal variant of AD (FvAD) [5]. Each of these variants of AD syndromes presents with a relative preservation of memory in addition to characteristic syndromes, including visuospatial deficits, aphasia, and executive dysfunction. Previous studies have demonstrated significant left hemisphere hypometabolism using 2-deoxy-2-[18]fluoro-D-glucose ([18F]FDG) positron-emission tomography (PET) in LPA patients; however, bilateral and symmetric uptake was observed with 2-(4′-[11C]methylaminophenyl)-6-hydroxybenzothiazole ([11C]PIB) PET imaging. In PCA, [18F]FDG PET imaging often revealed prominent hypometabolism in the parietal and occipital cortex [6]. Although frontal variant AD has been incorporated into new AD diagnostic criteria, little is known about the hypometabolism and amyloid deposition patterns and their involvement in brain networks.

In particular brain regions, variable syndromes may be correlated to the pattern of interactions between networks and pre-existing vulnerable molecular substrates [7]. Aβ and tau are two main pathogenic proteins resulting in AD pathology. The interaction of Aβ and tau enhances the potential for phenotypic variation. Stated by the emerging network paradigm of neurodegenerative disease, AD pathology relevant to different phenotypic is distributed along network connections [8–10]. As a result, the pathophysiology of AD may lead to a specific network vulnerability. In several studies, it has been demonstrated that regions composing the default mode network (DMN) showed a striking overlap with high levels of Aβ deposition in typical AD patients [11]. According to the previous study, it has been proposed that Aβ pathology may be associated with network cascading failure. It has not been completely understood those factors that initiate and drive this diversity. However, it may become more significant in understanding the pathophysiology of typical and variants of AD, with differential diagnosis, patient monitoring, and the design of targeted therapies for variant forms of AD [12].

To our knowledge, only few studies have focused on the pathogenic roles of Aβ plaques in variants of AD and how this is involved in brain networks. In this study, we hypothesized that variants of AD syndromes correlated with different network dysfunctions and that Aβ deposition in the most vulnerable network was different between typical and three types of AD variants.

Materials and Methods

Study Design and Subjects

In this prospective cohort study, AD patients and healthy control subjects were screened at the Tianjin Medical University General Hospital (TMUGH) and Tianjin Huanhu Hospital (Tianjin, China). Between 2012 and 2017, patients were enrolled using the IWG-2 criteria. All patients underwent neurologic examination and neuropsychological assessment with a battery of tests. Clinical diagnosis was established by experienced neurologists. Exclusion criteria included a history of major psychiatric or neurological (other than AD) illnesses, drug and/or alcohol abuse, and major vascular events. A magnetic resonance imaging (MRI) scan was performed to exclude structural abnormalities in AD and healthy control subjects.

Parametric images of [11C]PIB were assessed visually by two independent experienced nuclear medicine physicians. Scans were visually read as positive or negative for cortical PIB. Images were considered positive if [11C]PIB uptake was substantially greater in cortex (e.g., frontal, parietal, temporal, or occipital) and striatum than in white matter. Consequently, 29 [11C]PIB-negative patients were excluded, resulting in 65 AD patients for analysis, including 13 FvAD patients, 8 LPA patients, 6 PCA patients, and 38 TAD patients. The clinical follow-up period was 1 to 5 years after PET scans. Age-matched healthy control subjects were recruited and had normal neurologic examination results. None of the healthy control subjects had a history of neurologic, cardiovascular, or psychiatric conditions and all were [11C]PIB negative. This study was approved by the Ethics Committee of TMUGH. Written informed consent was obtained from each subject.

Neuropsychological Testing

Within 2 weeks prior to PET imaging, subjects underwent a battery of tests, which included Minimum Mental State Examination (MMSE), Montreal Cognitive Assessment (MoCA), Activity of Daily Living Scale (ADL), and Clinical Dementia Rating (CDR).

PET Imaging Acquisition

All participants underwent [18F]FDG and [11C]PIB PET imaging, which were conducted at the PET/X-ray computed tomography (CT) center of TMUGH with a GE Discovery LS PET/CT scanner in the three-dimensional scanning

mode. Subjects fasted for at least 6 h prior to tracer injection, so that their plasma glucose level was within the normal range (< 11.1 mmol/l). In addition, all subjects underwent [11C]PIB PET and [18F]FDG PET scanning using the same PET system on the same day. Both types of scanning were performed under resting conditions with the eyes closed, ambient noise, and dimmed light. For each acquisition, the subject's head was restricted by a head holder and was regularly checked during the PET scans using laser beams. [11C]PIB was injected into an antecubital vein as a bolus injection, with a mean dose of 370–555 MBq. [11C]PIB PET scans were acquired during a 90 min dynamic PET scan (34 frames: 4 × 15 s, 8 × 30 s, 9 × 60 s, 2 × 180 s, 8 × 300 s, 3 × 600 s). At a minimum of 2 h after [11C]PIB injection, subjects were injected [18F]FDG. They were intravenously injected with 259 MBq of [18F]FDG and a 10-min static PET scan was performed 40 min after injection. Each frame yielded 35 slices of 4.25-mm thickness, which covered the entire brain. Images were reconstructed to 128 × 128 matrix (pixel size of 2.5× 2.5 mm^2).

[18F]FDG Voxel-Wise Group Analysis

Voxel-based statistical analysis was performed using Statistical Parametric Mapping8 (SPM8) and Matlab2010b for Windows. Two-sample *t* tests and *T* contrasts were performed. A significance threshold of $p < 0.05$ corrected with an extent threshold of 50 voxels for multiple comparisons (family-wise error) was applied when comparing each AD group vs. healthy controls. In addition, a significance threshold of $p < 0.001$ was considered when directly comparing between patient groups. Anatomical localization was based on the superimposition of SPM-T maps onto the ch2bet template brain and identification of the localization using AAL software and anatomical atlases (http://www.talairach.org/). The findings were rendered using publicly available MRIcron software (http://www.sph.sc.edu/comd/rorden/mricron/).

Goodness of Fit Calculation

In each AD group, spatial overlap between hypometabolism patterns and the functional network was calculated by GOF. In brief, the highest GOF score template was selected as VOI for each AD group. The Stanford Functional Imaging in Neuropsychiatric Disorders Lab published functional network templates which were downloaded from the website: http://findlab.stanford.edu/functional_ROIs.html [13]. We have the access to a total of 15 network templates which include dorsal and ventral default mode network, precuneus network, primary and higher visual networks, visuospatial network, left and right language networks, left and right executive control networks, anterior and posterior salience networks, sensorimotor network, auditory network, and basal ganglia network. The GOF equals to z_{inside} minus $z_{outside}$. In this equation, z_{inside} stands for the mean *z* score of all voxels of the region of interest of the transformed voxel-wise *t*-map that fell inside the network template, and $z_{outside}$ is the mean z-score of all voxels outside the network template.

Analysis of [11C]PIB Uptake

Kinetic evaluations of [11C]PIB uptake were performed using PMOD software (version 3.7, PMOD Technologies Ltd., Zurich, Switzerland). In brief, volume of interests (VOIs) were delineated from [11C]PIB parametric non-displaceable binding potential (BPND) images, which were produced by application of the simplified reference tissue model (RPM2) that was a fully quantitative method to access data [14]. A quantitative measure of specific binding named BPND stands for the concentration of a specifically bound tracer relative to the concentration of free and non-specifically bound tracer in tissue under equilibrium conditions [15]. Cerebellar gray matter lacks Congo Red-positive and thioflavin-S-positive plaques and was therefore chosen as a reference tissue [16]. Image data of 35–90 min post injection were used for analysis of [11C]PIB uptake. [11C]PIB uptake was calculated from the time-activity curves of the template VOIs, and parametric images of BP_{ND} of [11C]PIB were generated.

Statistical Analyses

Statistical analyses were carried out using SPSS 13.0 software (SPSS Inc., Chicago, IL, USA). The comparison of demographic and clinical variables among AD groups was performed using one-way analysis of variance (ANOVA) and the chi-square test. Statistical analysis of BP_{ND} was performed using an analysis of covariance model that included age, sex, disease duration, and education as covariates. $p < 0.05$ was considered statistically significant.

Results

Demographic and Clinical Characteristics

The demographic and clinical characteristics of all participants are presented in Table 1. No significant differences between AD groups and the control group were observed in age, sex, years of education, age of onset, disease duration, and ADL score ($p > 0.05$). MMSE score and MoCA score in the control group were higher than each AD group ($p < 0.05$). The CDR score in the control group was lower compared to that of each AD group ($p < 0.05$).

Table 1. Demographic and clinical characteristics of participants

	FvAD	LPA	PCA	TAD	NC	*P* value[a]
Number	13	8	6	38	20	/
Sex (male/female)	4/9	3/5	4/2	14/24	11/9	/
Age[b] (year)	68.0 ± 3.4	68.8 ± 9.3	59.6 ± 4.2	67.0 ± 3.5	65.2 ± 9.5	0.043
Education level (year)	9.0 ± 2.7	11.5 ± 4.8	10.1 ± 2.9	11.6 ± 3.6	12.2 ± 4.0	0.023
Age of onset (year)	64.5 ± 3.0	64.5 ± 9.0	56.8 ± 3.4	65.3 ± 3.7	/	0.013
Duration[c] (month)	40.3 ± 19.0	51.0 ± 6.0	38.4 ± 19.7	20.4 ± 11.7	/	0.038
MMSE	17.0 ± 5.6	10.5 ± 6.1	19.6 ± 4.8	17.6 ± 9.6	29.6 ± 0.9	0.002
ADL	36.0 ± 15.6	44.3 ± 17.2	25.8 ± 11.1	31.8 ± 9.8	20.0 ± 0.0	0.068
CDR	1.2 ± 0.4	1.6 ± 0.8	0.6 ± 0.2	1.1 ± 0.5	0.0 ± 0.0	<0.001
MoCA	10.7 ± 5.2	5.8 ± 3.9	13.7 ± 5.9	8.4 ± 5.9	28.2 ± 1.9	<0.001

Data are the mean ± standard deviation unless specified otherwise
[a]One-way analysis of variance across groups (except sex and CDR)
[b]Age at time of PET scan
[c]Time between first symptoms and PET scan
Abbreviations: *FvAD* frontal variant of Alzheimer's disease, *LPA* logopenic variant primary progressive aphasia, *PCA* posterior cortical atrophy, *TAD* typical Alzheimer's disease, *NC* normal control, *MMSE* Minimum Mental State Examination, *MoCA* Montreal Cognitive Assessment, *ADL* Activity of Daily Living Scale, *CDR* Clinical Dementia Rating

[18F]FDG Voxel-Wise Group Results

Compared with control subjects, all AD groups showed hypometabolism in the inferior parietal lobule, middle and inferior temporal gyrus, and the precuneus/posterior cingulated gyrus. These regions were asymmetric involvement of the left side in LPA, including the left superior temporal gyrus. The bilateral dorsolateral frontal lobe and medial prefrontal cortex were reduced in FvAD. In addition, the metabolism was decreased in the temporal-parieto-occipital cortex in PCA (Fig. 1).

When comparing patient groups, patients with FvAD demonstrated a reduced metabolism in medial prefrontal cortex when compared with TAD. Moreover, patients with PCA showed greater hypometabolism in the right occipital lobe when compared with TAD. In addition, patients with TAD showed a reduced metabolism in the right inferior parietal lobule and middle temporal gyrus when compared with LPA (Fig. 2).

GOF Analysis of [18F]FDG Voxel-Wise t-Maps Overlapping with Functional Network Templates

The hypometabolism patterns demonstrated that the most vulnerable network was the left executive control network (GOF score = 4.3, 5.0) in TAD and FvAD. For LPA, the highest GOF score (1.9) belonged to the auditory network,

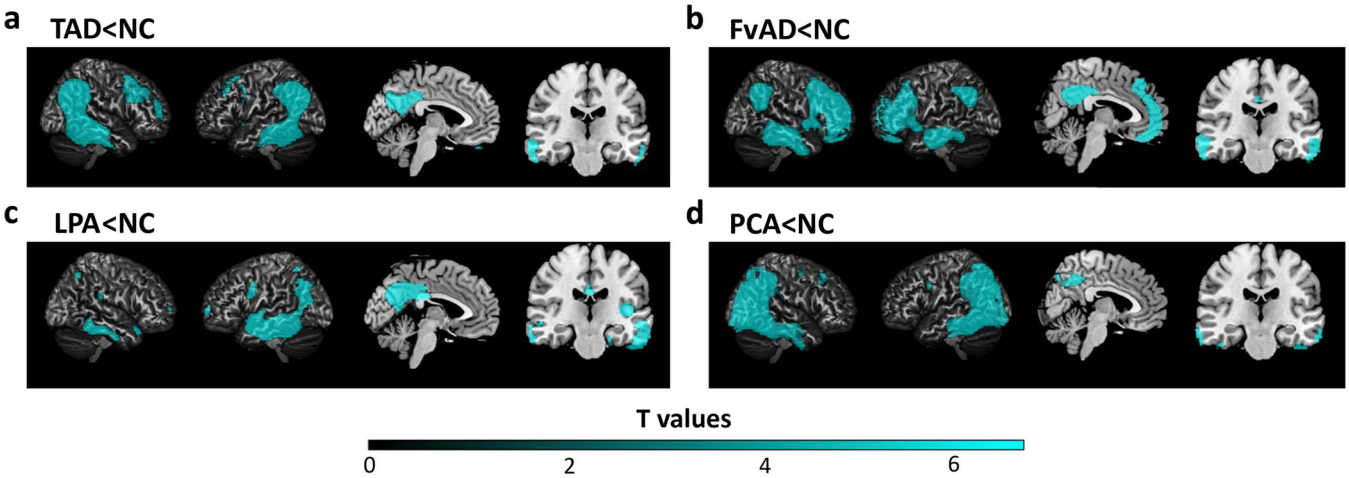

Fig. 1. Patterns of [18F]FDG in four types of AD compared with normal controls (NC). **a** TAD and NC. **b** FvAD and NC. **c** LPA and NC. **d** PCA and NC. Shown are *t*-maps after correction for multiple comparisons (FWE at $p < 0.05$) rendered on the ch2bet template brain. A cyan color in the [18F]FDG maps indicates a lower [18F]FDG uptake in each patient group compared with NC group. Each AD group showed hypometabolism in the inferior parietal lobule, middle and inferior temporal gyrus, and precuneus/posterior cingulated gyrus. **b** The bilateral dorsolateral frontal lobe and medial prefrontal cortex were reduced in FvAD. **c** These regions were asymmetric involvement of left side in LPA, including left superior temporal gyrus. **d** The metabolism was decreased in the temporal-parieto-occipital cortex in PCA.

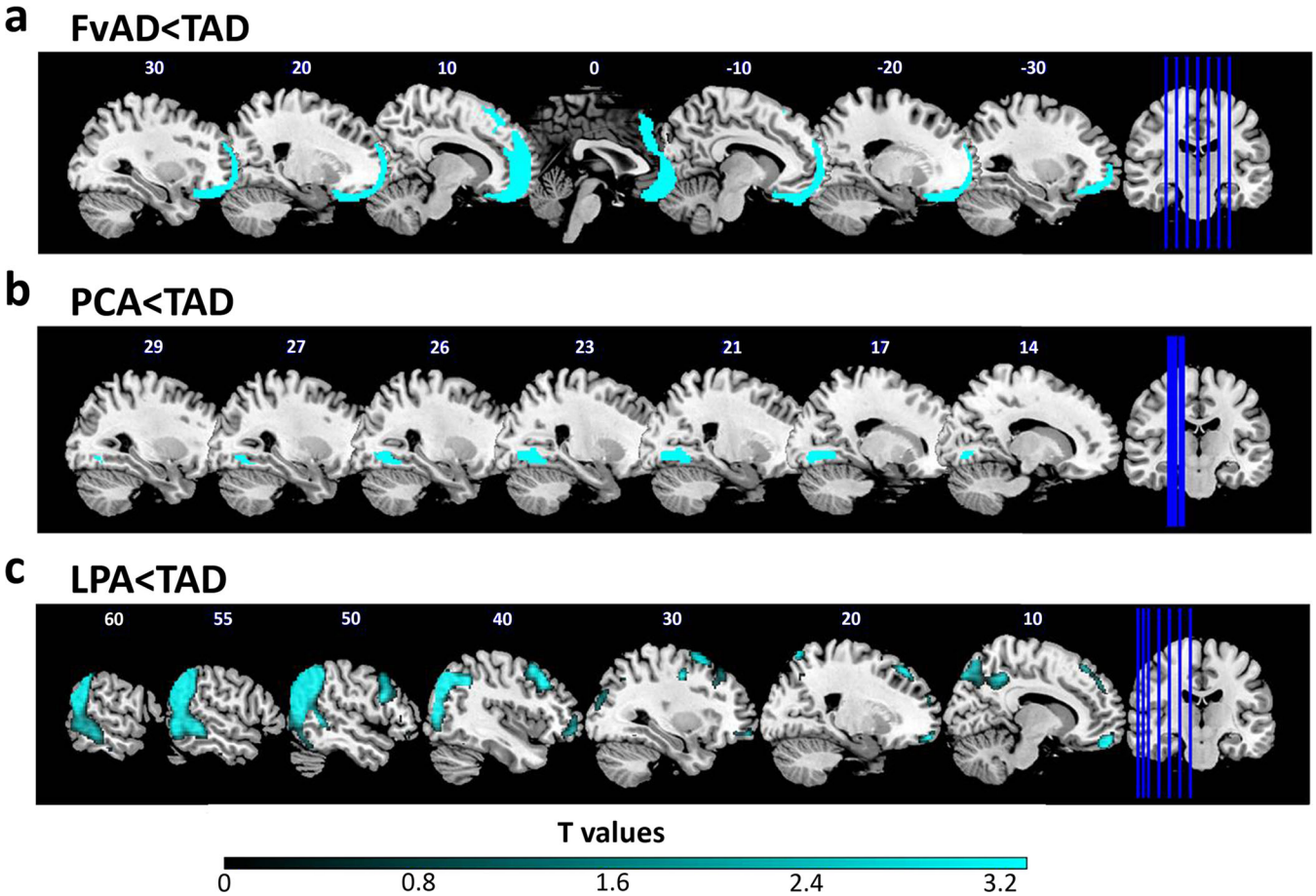

Fig. 2. Differences in [18F]FDG uptake between **a** FvAD and TAD, **b** PCA and TAD, and **c** LPA and TAD. Shown are *t*-maps with a significance threshold of $p < 0.001$ rendered on the ch2bet template brain. A cyan color in the [18F]FDG maps indicates a lower [18F]FDG uptake in FvAD and PCA compared with TAD, and in TAD compared with LPA. The patient group with FvAD showed a reduced metabolism in the medial prefrontal cortex compared with TAD. Patients with PCA showed a greater hypometabolism in the right occipital lobe compared with TAD. Patients with TAD showed a reduced metabolism in the right inferior parietal lobule and middle temporal gyrus compared with LPA.

whereas for PCA, the highest visual network was the most vulnerable (GOF score = 6.0) (Fig. 3).

[11C]PIB Uptake in Functional Network Templates

Figure 4 presents the [11C]PIB uptake results in three specific functional network templates for each group. Our data showed that [11C]PIB BP_{ND} did not differ among AD groups in any of these networks ($p > 0.05$).

Discussion

In this study, we investigated the hypometabolism patterns, network changes, and amyloid deposition quantities across TAD and three phenotypes of atypical AD, including FvAD, PCA, and LPA. Our findings showed that (1) all AD groups associated with a largely overlapping pattern of hypometabolism that was centered in the temporoparietal region and the retrosplenial cortex and (2) hypometabolism patterns demonstrated that involvement of the left executive-control network (ECN) would be specific to both TAD and FvAD. Moreover, the involvement of the auditory and higher visual networks would be specific to LPA and PCA, respectively. These findings matched the clinical profile of patients, and (3) for upstream amyloid pathological changes, no differences were observed among all groups in any network.

In this study, we directly compared the specific distribution of hypometabolism in four AD syndromes at presentation and showed largely overlapping damage to the temporoparietal region and the retrosplenial cortex. This suggested that the involvement of these regions is a common feature in both TAD and variant AD syndromes. Moreover, around these large regions of common hypometabolism, small distinctive regions were associated with variant AD syndromes. Consistent with their greater executive difficulties, FvAD showed that the bilateral dorsolateral frontal lobe and the medial prefrontal cortex were reduced. In addition,

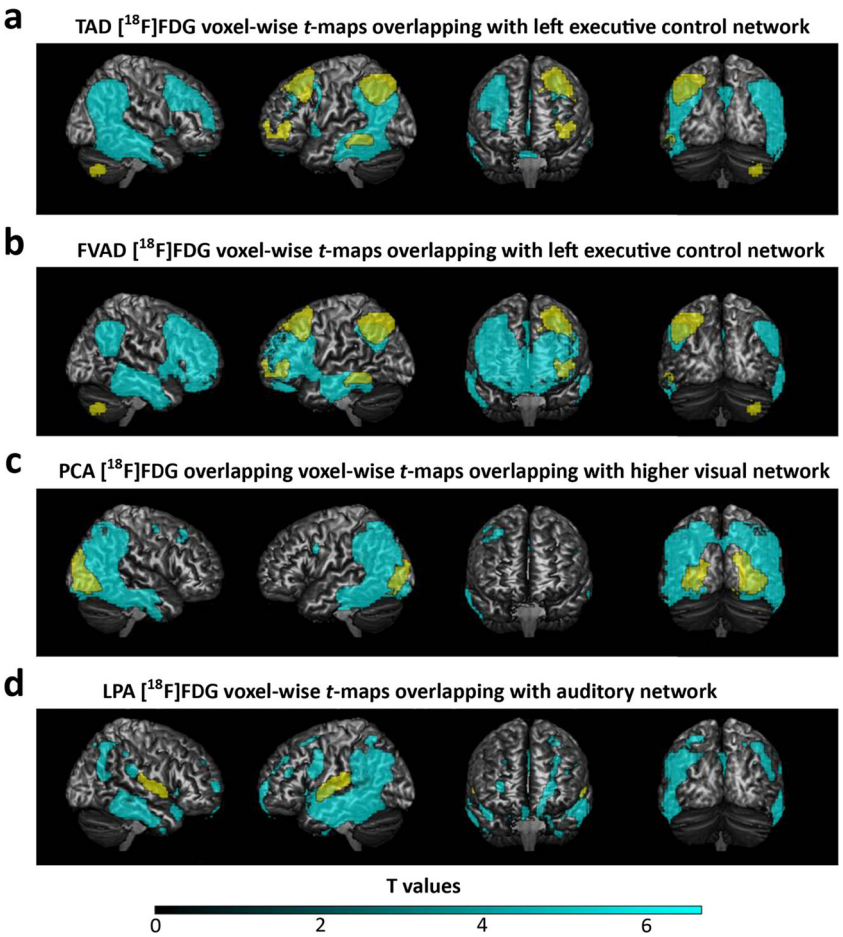

Fig. 3. Overlap maps showing that each [18F]FDG SPM-T map correlates with the best-fitting network template. A cyan color in the [18F]FDG maps indicated lower [18F]FDG uptake in each patient group compared with NC group, whereas a yellow color represents the best fit network template. **a**, **b** The hypometabolism patterns found the most vulnerable network was the left executive-control network (GOF score = 4.3, 5.0) in TAD and FvAD. **c** For PCA, the higher visual network was the most vulnerable (GOF score = 6.0). **d** For LPA, the highest GOF score (1.9) belonged to auditory network.

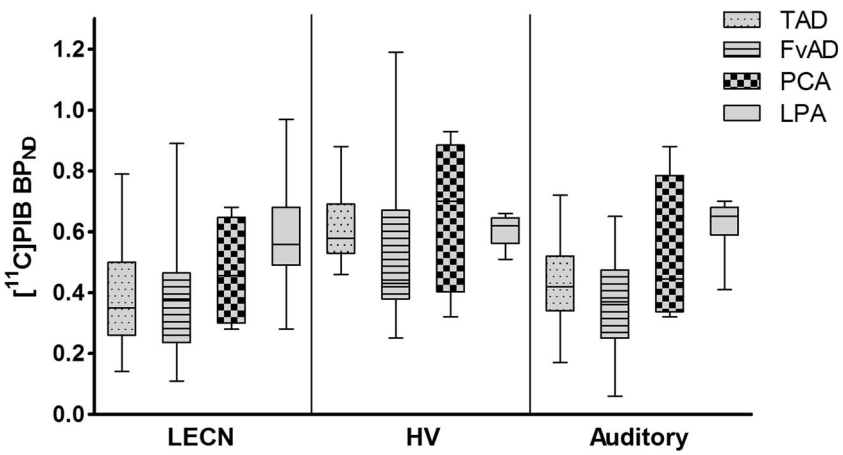

Fig. 4. [11C]PIB BP_{ND} in TAD, LPA, FvAD, and PCA in specific functional network templates. No differences were observed among Alzheimer's disease (AD) groups in any of these networks ($p > 0.05$). Abbreviations: LECN, left executive control networks; HV, higher visual network; Auditory, auditory network.

LPA showed greater left superior, middle, and inferior temporal gyrus hypometabolism, which was compatible with their greater language comprehension and production deficits. PCA showed greater hypometabolism in the right occipital lobe compared with TAD, in keeping with their visual disturbance. Thus, our study is consistent with previous MRI and [18F]FDG PET findings on behavioral/dysexecutive, language, and visuospatial AD presentation [17–19].

Glucose metabolism is a complex phenomenon reflecting multiple metabolic processes. It is clearly related to synapse structure and function as well as measures of brain function and connectivity using multiple modalities [20]. Based on these hypometabolism patterns, [18F]FDG analyses provided converging evidence implicating differential involvement of specific networks in each clinical variant of AD. The most distinct pattern was found in PCA. Consistent with previously reported findings, the region of hypometabolism patterns showed the best fit with higher visual networks [6]. PCA is a focal neurodegenerative disorder of higher visual processing and spatial praxis with relative sparing of memory and insight. These findings matched the clinical profile of AD. Although frontal variant AD has been incorporated into new AD diagnostic criteria, little is known about the hypometabolism patterns and how it involves with brain networks. FvAD refers to clinical presentation of predominantly behavioral and/or dysexecutive deficits, disinhibition, and preservative/stereotypical behaviors, and may mimic that of behavioral variant frontotemporal dementia (bvFTD). This is illustrated by the 10–40 % of patients who are clinically diagnosed with bvFTD and are found to have AD pathology based on amyloid PET scans or post-mortem evaluation [21, 22]. Our findings suggested that frontal variant AD showed specific frontal lobe metabolic reduction, which fit left ECN best. Previous studies that focused on fMRI studies indicated that the executive network had historically been associated with regions in the parietal lobe, dorsal lateral prefrontal cortex, the middle frontal gyrus, and contra lateral cerebellar areas [13]. The left ECN deficit in FvAD could explain the distinct executive difficulties. Patients with TAD also demonstrated the best fit with the left ECN. The GOF score in FvAD was higher compared to that in TAD, indicating that left ECN was more destroyed in FvAD compared to TAD. Our results revealed that the best fit network with LPA was the auditory network, which was inconsistent with the findings reported in a previous [18F]FDG PET study [6]. LPA is characterized by a slow speech, sentence repetition, lexical and grammatical comprehension, single word retrieval and fluency, and spontaneous speech. Associated with a phonological loop disorder which was the core cognitive deficit in LPA, an MRI study showed that LPA was impaired in the domains of auditory input processing, repetition, and working memory [23]. Moreover, an auditory-verbal short-term memory deficit had been hypothesized to be the critical mechanism underpinning the LPA syndrome [24]. This hypothesis was based on neuropsychological evidence of digit span, sentence repetition, and syntactic comprehension deficits (affecting both simple and complex sentence constructions) and neuroimaging evidence of the left posterior temporal and inferior parietal atrophy. The association of these regions with the auditory-verbal short-term memory as presented previously strengthened our findings of auditory network as the best fit [25]. It is important for clarifying cognitive deficit and progression to AD by metabolic brain networks' alterations [20].

In the current study, we revealed that amyloid deposition was diffusely distributed over the entire cortex and that no significant differences in [11C]PIB retention were found in the specific networks among AD syndromes. Currently, only few multimodal imaging studies are available that compared amyloid deposition underline with specific networks. Previous studies that focused on PPA showed that the distribution of amyloid pathology (as measured by [11C]PIB or at autopsy) in AD-associated cases was indistinguishable from that found in TAD [23, 26]. The distribution of amyloid in PCA is controversial, and several studies demonstrating higher numbers of amyloid plaques in primary and associated visual cortex in PCA compared to TAD, whereas others did not find differences in the distribution of amyloid pathology [27]. Reasons for discrepant findings between this and other [11C]PIB studies may include differences in sample size, group composition, and methodological differences. It is not accepted that Aβ has a directly detrimental impact on neuronal function. However, it is commonly believed that Aβ results in neuronal dysfunction and neuron death *via* tau pathology [28]. In line with this notion, glucose hypometabolism has been demonstrated to show a stronger correlation with neurofibrillary tangles compared to Aβ plaque burden *in vivo* and postmortem [29, 30]. Another recent advancement in the field suggested that tau may exhibit properties similar to those of prions [31]. These recent studies showed that in brain regions, it was mainly observed that tau pathology was relevant to clinical symptoms and overlapped with glucose metabolism decreasing area [32]. Tau PET imaging may be used as a critical biomarker for displaying neuronal deficit regions *in vivo* and may help to establish the patterns of AD variants. In addition, in recent years, a third pathogenic component is gaining strength in the onset and progression of AD, the neuroinflammatory response mediated primarily by the brain's resident immune cells, microglia. Some latest studies show that microglia are highly stimulated by Aβ and might be mediated by the accumulation of toxic phospho-tau species; in consequence, it could be implicated in the neurodegenerative process [33].

Limitations

Although promising, our study has several limitations. First, autopsy confirmation of AD was not available in any of our

subjects, although our selection criteria were strictly followed with IWG-2 criteria to maximize the likelihood of underlying AD pathology. Second, the sample size of each AD group was small. Therefore, any findings from this study may be limited by the small sample size. Third, there is still debate over the appropriate threshold for defining Aβ positivity and here we defined [11C]PIB positivity by visual analysis rather than on quantitation. We reviewed previous literatures which compared the visual interpretation with quantitative evaluation of [11C]PIB PET [34]. The quantitative method may facilitate correct diagnosis in low-level amyloid cases. As a previous study showed that this proportion was small, the impact on the conclusions may be a little. Fourth, [18F]FDG PET is an indirect way to identify functional neural networks, in spite of relating to synaptic activity and being used to access brain function. On the other hand, further studies by using both task-free and task-dependent functional MRI method may directly elucidate the role of different functional networks in AD variants. Finally, another limitation is the GOF network analysis, which may or may not be good enough to identify brain networks. Multiple variate analysis, such as spatial covariate analysis may be more beneficial. Therefore, further studies are needed.

Conclusions

The phenotypic diversity of AD correlates with specific functional network failure. However, Aβ plaques do not associate with specific network vulnerability.

Acknowledgements. The study was supported by the National Natural Science Foundation of China (Grant NO. 81571057 and 81501035), Tianjin Science and Technology Project (Grant NO. 16ZXMJSY00010).

Compliance with Ethical Standards. This study was approved by the Ethics Committee of Tianjin Medical University General Hospital (IRB2014–071-01).

Conflict of Interest Statement

The authors declare that they have no conflict of interest.

References

1. Kelley BJ, Petersen RC (2007) Alzheimer's disease and mild cognitive impairment. Neurol Clin 25:577–609
2. Braak H, Braak E (1991) Neuropathological stageing of Alzheimer-related changes. Acta Neuropathol 82:239–259
3. Thal DR, Rub U, Orantes M, Braak H (2002) Phases of a beta-deposition in the human brain and its relevance for the development of AD. Neurology 58:1791–1800
4. Minoshima S, Giordani B, Berent S, Frey KA, Foster NL, Kuhl DE (1997) Metabolic reduction in the posterior cingulate cortex in very early Alzheimer's disease. Ann Neurol 42:85–94
5. Dubois B, Feldman HH, Jacova C, Hampel H, Molinuevo JL, Blennow K, DeKosky ST, Gauthier S, Selkoe D, Bateman R, Cappa S, Crutch S, Engelborghs S, Frisoni GB, Fox NC, Galasko D, Habert MO, Jicha GA, Nordberg A, Pasquier F, Rabinovici G, Robert P, Rowe C, Salloway S, Sarazin M, Epelbaum S, de Souza LC, Vellas B, Visser PJ, Schneider L, Stern Y, Scheltens P, Cummings JL (2014) Advancing research diagnostic criteria for Alzheimer's disease: the IWG-2 criteria. Lancet Neurol 13:614–629
6. Lehmann M, Ghosh PM, Madison C, Laforce R Jr, Corbetta-Rastelli C, Weiner MW, Greicius MD, Seeley WW, Gorno-Tempini ML, Rosen HJ, Miller BL, Jagust WJ, Rabinovici GD (2013) Diverging patterns of amyloid deposition and hypometabolism in clinical variants of probable Alzheimer's disease. Brain 136:844–858
7. Jones DT, Knopman DS, Gunter JL, Graff-Radford J, Vemuri P, Boeve BF, Petersen RC, Weiner MW, Jack CR Jr, Alzheimer's Disease Neuroimaging Initiative (2016) Cascading network failure across the Alzheimer's disease spectrum. Brain 139:547–562
8. Pievani M, de Haan W, Wu T, Seeley WW, Frisoni GB (2011) Functional network disruption in the degenerative dementias. Lancet Neurol 10:829–843
9. Zhou J, Greicius MD, Gennatas ED, Growdon ME, Jang JY, Rabinovici GD, Kramer JH, Weiner M, Miller BL, Seeley WW (2010) Divergent network connectivity changes in behavioural variant frontotemporal dementia and Alzheimer's disease. Brain 133:1352–1367
10. Raj A, Kuceyeski A, Weiner MA (2012) A network diffusion model of disease progression in dementia. Neuron 73:1204–1215
11. Buckner RL, Sepulcre J, Talukdar T et al (2009) Cortical hubs revealed by intrinsic functional connectivity: mapping, assessment of stability and relation to Alzheimer's disease. Neurobiol Dis 29:1860–1873
12. Warren JD, Fletcher PD, Golden HL (2012) The paradox of syndromic diversity in Alzheimer disease. Nat Rev Neurol 8:451–464
13. Shirer WR, Ryali S, Rykhlevskaia E, Menon V, Greicius MD (2012) Decoding subject-driven cognitive states with whole-brain connectivity patterns. Cereb Cortex 22:158–165
14. Wu Y, Carson R (2002) Noise reduction in the simplified reference tissue model for neuroreceptor functional imaging. J Cereb Blood Flow Metab 22:1440–1452
15. Yaqub M, Tolboom N, Boellaard R, van Berckel BNM, van Tilburg EW, Luurtsema G, Scheltens P, Lammertsma AA (2008) Simplified parametric methods for [11C]PIB studies. NeuroImage 42:76–86
16. Yamaguchi H, Hirai S, Morimatsu M, Shoji M, Nakazato Y (1989) Diffuse type of senile plaques in the cerebellum of Alzheimer-type dementia. Acta Neuropathol 77:314–319
17. Woodward MC, Rowe CC, Jones G, Villemagne VL, Varos TA (2015) Differentiating the frontal presentation of Alzheimer's disease with FDG-PET. J Alzheimers Dis 44:233–242
18. Matías-Guiu JA, Cabrera-Martín MN, Pérez-Castejón MJ, Moreno-Ramos T, Rodríguez-Rey C, García-Ramos R, Ortega-Candil A, Fernandez-Matarrubia M, Oreja-Guevara C, Matías-Guiu J, Carreras JL (2015) Visual and statistical analysis of 18F-FDG PET in primary progressive aphasia. Eur J Nucl Med Mol Imaging 42:916–927
19. Leyton CE, Hodges JR, Piguet O, Ballard KJ (2017) Common and divergent neural correlates of anomia in amnestic and logopenic presentations of Alzheimer's disease. Cortex 86:45–54
20. Arnemann KL, Stöber F, Narayan S et al (2017) Metabolic brain networks in aging and preclinical Alzheimer's disease. Neuroimage Clin 17:987–999
21. Rabinovici GD, Rosen HJ, Alkalay A, Kornak J, Furst AJ, Agarwal N, Mormino EC, O'Neil JP, Janabi M, Karydas A, Growdon ME, Jang JY, Huang EJ, DeArmond SJ, Trojanowski JQ, Grinberg LT, Gorno-Tempini ML, Seeley WW, Miller BL, Jagust WJ (2011) Amyloid vs FDG-PET in the differential diagnosis of AD and FTLD. Neurology 77:2034–2042
22. Beach TG, Monsell SE, Phillips LE, Kukull W (2012) Accuracy of the clinical diagnosis of Alzheimer disease at National Institute on Aging Alzheimer Disease Centers, 2005-2010. J Neuropathol Exp Neurol 71:266–273
23. Gorno-Tempini ML, Brambati SM, Ginex V, Ogar J, Dronkers NF, Marcone A, Perani D, Garibotto V, Cappa SF, Miller BL (2008) The logopenic/phonological variant of primary progressive aphasia. Neurology 71:1227–1234
24. Gorno-Tempini ML, Dronkers NF, Rankin KP, Ogar JM, Phengrasamy L, Rosen HJ, Johnson JK, Weiner MW, Miller BL (2004) Cognition and anatomy in three variants of primary progressive aphasia. Ann Neurol 55:335–346
25. Foxe D, Leyton CE, Hodges JR, Burrell JR, Irish M, Piguet O (2016) The neural correlates of auditory and visuospatial span in logopenic progressive aphasia and Alzheimer's disease. Cortex 83:39–50

26. Mesulam M, Wicklund A, Johnson N, Rogalski E, Léger GC, Rademaker A, Weintraub S, Bigio EH (2008) Alzheimer and frontotemporal pathology in subsets of primary progressive aphasia. Ann Neurol 63:709–719
27. Rosenbloom MH, Alkalay A, Agarwal N, Baker SL, O'Neil JP, Janabi M, Yen IV, Growdon M, Jang J, Madison C, Mormino EC, Rosen HJ, Gorno-Tempini ML, Weiner MW, Miller BL, Jagust WJ, Rabinovici GD (2011) Distinct clinical and metabolic deficits in PCA and AD are not related to amyloid distribution. Neurology 76:1789–1796
28. Jack CR Jr, Knopman DS, Jagust WJ et al (2013) Tracking pathophysiological processes in Alzheimer's disease: an updated hypothetical model of dynamic biomarkers. Lancet Neurol 12:207–216
29. Ossenkoppele R, Schonhaut DR, Baker SL, O'Neil JP, Janabi M, Ghosh PM, Santos M, Miller ZA, Bettcher BM, Gorno-Tempini ML, Miller BL, Jagust WJ, Rabinovici GD (2015) Tau, amyloid, and hypometabolism in a patient with posterior cortical atrophy. Ann Neurol 77:338–342
30. Rapoport SI, Horwitz B, Grady CL et al (1991) Abnormal brain glucose metabolism in Alzheimer's disease, as measured by position emission tomography. Adv Exp Med Biol 29:231–248
31. Josephs KA (2017) Current understanding of neurodegenerative diseases associated with the protein tau. Mayo Clin Proc 92:1291–1303
32. Dronse J, Fliessbach K, Bischof GN, von Reutern B, Faber J, Hammes J, Kuhnert G, Neumaier B, Onur OA, Kukolja J, van Eimeren T, Jessen F, Fink GR, Klockgether T, Drzezga A (2017) In vivo patterns of tau pathology, amyloid-β burden, and neuronal dysfunction in clinical variants of Alzheimer's disease. J Alzheimers Dis 55:465–471
33. Gutierrez A, Vitorica J (2018) Toward a new concept of Alzheimer's disease models: a perspective from neuroinflammation. J Alzheimers Dis:1–10
34. Yamane T, Ishii K, Sakata M et al (2017) Inter-rater variability of visual interpretation and comparison with quantitative evaluation of ^{11}C-PiB PET amyloid images of the Japanese Alzheimer's Disease Neuroimaging Initiative (J-ADNI) multicenter study. Eur J Nucl Med Mol Imaging 44:850–857